Appl Compos Mater (2016) 23:45–69
DOI 10.1007/s10443-015-9449-0

Finite Element Analysis of 2.5D Woven Composites, Part II: Damage Behavior Simulation and Strength Prediction

Jian Song[1,2] · **Weidong Wen**[1] · **Haitao Cui**[1] · **Hongjian Zhang**[1] · **Ying Xu**[1]

Received: 30 April 2015 / Accepted: 13 May 2015 / Published online: 9 June 2015

Abstract In the first part of the work, a new 2.5D woven composites finite element model (2.5D WCFEM) which took into consideration the impact of face structures and can accurately predict the main elastic performances has been established. In this part, the stress–strain behavior and the damage characteristic of this material under uniaxial tension are simulated using nonlinear progressive damage analysis based on damage mechanics. Meanwhile, experimental investigation and fracture analysis are conducted to evaluate the validity of the proposed method. Finally, the influence of woven parameters on the mechanical behavior is discussed. Compared with the test results, a good agreement between the computational and experimental results has been obtained. The progressive damage characteristic and main failure modes are also revealed.

Keywords 2.5D woven composites · Damage characteristic · Finite element analysis · Damage characteristic · Experiment

1 Introduction

2.5D angle-interlock woven composites as a new class of textile composites have a great deal of advantages over the conventional laminated composites, including near-net-shape, better out-of-plane stiffness and strength etc. However, owing to their high anisotropic nature, it is difficult to fully predict their mechanical characteristic and damage mechanism. Compared to 3D woven or braided composites, the technology of

✉ Jian Song
dfsongjian2006@126.com

[1] Nanjing University of Aeronautics and Astronautics Jiangsu Province Key Laboratory of Aerospace Power System, State Key Laboratory of Mechanics and Control of Mechanical Structures, Nanjing University of Aeronautics and Astronautics, Jiangsu 210016, China

[2] College of Energy and Power Engineering, Nanjing University of Aeronautics and Astronautics, Nanjing 210016, People's Republic of China

2.5D woven composites is more simply, and the engineering productions fabricated by this material have own of higher twisting degree.

Up to now, although 2.5D woven composite material has been successfully applied in the structure of aero-engine fan blade, the studies on mechanical behavior of material are focus on the elastic property [1–3], but the reports about damage behavior and strength prediction are still limited. Some experimental researches and numerical simulations have been conducted to study on the mechanical property of material [4–6]. The test results show that the stress–strain curve has an obvious nonlinear and the fracture surfaces exist amount of fiber breaking and delaminated damage modes in the warps. Additionally, the initial cracks occur at the crossing point in outermost layer wefts, but the extension degree of damage is not obvious until just prior to failure. Masaru [7] simulated the damage behavior of 2D woven composites by finite element method. Lu et al. [8] predicted the mechanical characteristic of 2.5D woven composites under uniaxial tension based on the multi-scale finite element analysis. Dong [9] studied the stiffness, strength and damage extended issues of 2.5D woven composites based on commercial finite element analysis software ANSYS.

Although some works have been done to investigate the mechanical behavior of 2.5D woven composites based on finite element method, majority of FE models have not taken the influence of outmost layer structure into consideration. Nevertheless, according to the investigation of 3D braided composites [10, 11], the face and corner cells have an obvious impact on the mechanical properties of braided composites. Therefore, it is required to establish a more precise model to study the mechanical characteristic, and the effect of outmost layer structure on the strength and mechanical behavior can be studied based on this FE model.

The present study (Part II) is focused on characterizing the damage behavior and predicting the strength of 2.5D woven composites under uniaxial tension in the warp and weft direction based on the progressive damage method (PDM). In Section 2, the theory foundation of PDM is derived in detail, and the related material performance reduction approach is proposed. Then, some numerical simulations based on PDM are performed, and the strength, stress–strain curves and damage process of material in the warp and weft directions are investigated. Finally, the influence of thickness and fiber aggregation density on the strength and stress–strain is discussed.

2 Damage Model and Mathematical Formulation

2.1 Theoretical Formulation of Constitutive Relationship

Owing to the complexity of geometric model, a progressive damage method (PDM) is used to investigate the damage behavior of 2.5D woven composites, which includes two main parts: fiber bundle and resin-rich matrix. In this article, fiber yarn and resin-rich matrix can be regarded macroscopically as anisotropic and isotropic homogeneous materials, respectively.

To characterize the damage modes of anisotropic material, the Murakami's damage tensor is introduced, and assuming that the reduction of effective loading for the damaged model is equivalent to the reduction of effective loading area for undamaged model. Therefore, the material damage state can be defined by the following Eq. (1)

$$\overline{\boldsymbol{\sigma}} = \boldsymbol{\sigma}(1-\boldsymbol{\omega})^{-1} \tag{1}$$

where $\overline{\boldsymbol{\sigma}}$ and $\boldsymbol{\sigma}$ are the damage stress tensor and undamaged stress tensor, respectively. $\boldsymbol{\omega}$ represents the damage tensor, which can be expressed as follows.

$$\boldsymbol{\omega} = \omega_i \mathbf{n_i} \otimes \mathbf{n_i}, \quad i = (1,2,3) \tag{2}$$

where ω_i and n_i are the principal value and principle unit vector of damage tensor, respectively. In order to derive the formulas more simply, define that

$$\boldsymbol{\varphi} = (1-\boldsymbol{\omega})^{-1} \tag{3}$$

Furthermore, owing to the asymmetry of damage stress tensor in most cases, therefore, an effective symmetric damage stress tensor $\widetilde{\boldsymbol{\sigma}}$ can be introduced and treaded by tensor form as follows.

$$\begin{aligned}
\widetilde{\boldsymbol{\sigma}} &= \frac{1}{2}\left(\overline{\boldsymbol{\sigma}} + \overline{\boldsymbol{\sigma}}^T\right) = \frac{1}{2}\left((\boldsymbol{\sigma}\cdot\boldsymbol{\varphi}) + (\boldsymbol{\sigma}\cdot\boldsymbol{\varphi})^T\right) \\
&= \frac{1}{2}\left(\boldsymbol{\sigma}\cdot\boldsymbol{\varphi} + \boldsymbol{\varphi}^T\cdot\boldsymbol{\sigma}^T\right) \\
&= \frac{1}{2}\left(\mathbf{I}\cdot\boldsymbol{\sigma}\cdot\boldsymbol{\varphi} + \boldsymbol{\varphi}\cdot\boldsymbol{\sigma}\cdot\mathbf{I}\right) \\
&= \frac{1}{2}\left[(\delta_{im}\mathbf{i}_i\mathbf{i}_m)\cdot(\sigma_{kl}\mathbf{i}_k\mathbf{i}_l)\cdot\left(\varphi_{nj}\mathbf{i}_n\mathbf{i}_j\right) + (\varphi_{in}\mathbf{i}_i\mathbf{i}_n)\cdot(\sigma_{kl}\mathbf{i}_l\mathbf{i}_k)\cdot\left(\delta_{mj}\mathbf{i}_m\mathbf{i}_j\right)\right] \\
&= \frac{1}{2}\left[\left(\delta_{im}\delta_{mk}\delta_{\ln}\sigma_{kl}\varphi_{nj}\mathbf{i}_i\mathbf{i}_j\right) + \left(\delta_{mj}\delta_{nl}\delta_{km}\sigma_{kl}\varphi_{in}\mathbf{i}_i\mathbf{i}_j\right)\right] \quad = \frac{1}{2}\left(\delta_{ik}\varphi_{lj} + \delta_{kj}\varphi_{il}\right)\sigma_{kl}\mathbf{i}_i\mathbf{i}_j
\end{aligned} \tag{4}$$

Next, a four-order tensor $\mathbf{M}(\boldsymbol{\omega})$ as follows.

$$\mathbf{M}(\omega) = M_{ijkl}\mathbf{i}_i\mathbf{i}_j\mathbf{i}_k\mathbf{i}_l = \frac{1}{2}\left(\delta_{ik}\varphi_{lj} + \delta_{kj}\varphi_{il}\right)\sigma_{kl}\mathbf{i}_i\mathbf{i}_j \tag{5}$$

Then, substitute Eq. (4) into Eq. (5), yields:

$$\widetilde{\boldsymbol{\sigma}} = \mathbf{M}(\omega) : \boldsymbol{\sigma} \tag{6}$$

Until now, the mapping relationship between the symmetric damage variable and asymmetric damage variable is derived and in matrix form, $\mathbf{M}(\boldsymbol{\omega})$ is expressed as follows.

$$\begin{Bmatrix} \overline{\sigma}_{11} \\ \overline{\sigma}_{22} \\ \overline{\sigma}_{33} \\ \overline{\sigma}_{23} = \overline{\sigma}_{32} \\ \overline{\sigma}_{13} = \overline{\sigma}_{31} \\ \overline{\sigma}_{12} = \overline{\sigma}_{21} \end{Bmatrix} = \begin{Bmatrix} \varphi_1 & 0 & 0 & 0 & 0 & 0 \\ 0 & \varphi_2 & 0 & 0 & 0 & 0 \\ 0 & 0 & \varphi_3 & 0 & 0 & 0 \\ 0 & 0 & 0 & \dfrac{\varphi_2+\varphi_3}{2} & 0 & 0 \\ 0 & 0 & 0 & 0 & \dfrac{\varphi_1+\varphi_3}{2} & 0 \\ 0 & 0 & 0 & 0 & 0 & \dfrac{\varphi_2+\varphi_3}{2} \end{Bmatrix} \begin{Bmatrix} \sigma_{11} \\ \sigma_{22} \\ \sigma_{33} \\ \sigma_{23} = \sigma_{32} \\ \sigma_{13} = \sigma_{31} \\ \sigma_{12} = \sigma_{21} \end{Bmatrix} \tag{7}$$

In addition, the constitutive equation of the damaged material can be defined by Eq. (8).

$$W = \frac{1}{2}\sigma_i\varepsilon_i = \frac{1}{2}\overline{\boldsymbol{\sigma}}^T : \boldsymbol{\varepsilon} = \frac{1}{2}\overline{\boldsymbol{\sigma}}^T : S : \overline{\boldsymbol{\sigma}} \tag{8}$$

where $\mathbf{S}$ is the flexibility matrix of material. Furthermore, according to the hypothesis of equivalent strain energy, the damage variable can be introduced into the constitutive equation, namely

$$W = \frac{1}{2}\tilde{\sigma}^T : \varepsilon = \frac{1}{2}\tilde{\sigma}^T : S : \tilde{\sigma} \quad = \frac{1}{2}(\mathbf{M}(\omega) : \overline{\sigma})^T : S : (\mathbf{M}(\omega) : \overline{\sigma})$$
$$= \frac{1}{2}\overline{\sigma} : \mathbf{M}(\omega)^T : S : \mathbf{M}(\omega) : \overline{\sigma} \quad = \frac{1}{2}\overline{\sigma} : \left[\left(\mathbf{M}(\omega)^{-1}\right) : S^{-1} : \left(\mathbf{M}(\omega)^T\right)^{-1}\right]^{-1} : \overline{\sigma} \tag{9}$$
$$= \frac{1}{2}\overline{\sigma} : \left[\left(\mathbf{M}(\omega)^{-1}\right) : S^{-1} : \left(\mathbf{M}(\omega)^{-1}\right)^T\right]^{-1} : \overline{\sigma} \quad = \frac{1}{2}\overline{\sigma}^T : \left[\mathbf{M}(\omega)^{-1} : C : \left(\mathbf{M}(\omega)^{-1}\right)^T\right]^{-1} : \overline{\sigma}$$

where **C** is the stiffness matrix of material. Thus, the stiffness tensors for the damage configuration can be obtained as follows.

$$\mathbf{C}(\omega) = \mathbf{M}(\omega)^{-1} : C : \left(\mathbf{M}(\omega)^{-1}\right)^T \tag{10}$$

Hence, the damaged stiffness matrix of yarn can be expressed by matrix formulation as follows.

$$[C] = \begin{bmatrix} \varphi_1 & 0 & 0 & 0 & 0 & 0 \\ 0 & \varphi_2 & 0 & 0 & 0 & 0 \\ 0 & 0 & \varphi_3 & 0 & 0 & 0 \\ 0 & 0 & 0 & \frac{\varphi_2+\varphi_3}{2} & 0 & 0 \\ 0 & 0 & 0 & 0 & \frac{\varphi_1+\varphi_3}{2} & 0 \\ 0 & 0 & 0 & 0 & 0 & \frac{\varphi_2+\varphi_3}{2} \end{bmatrix}^{-1} \cdot \begin{bmatrix} Q_{11} & Q_{12} & Q_{13} & 0 & 0 & 0 \\ & Q_{22} & Q_{23} & 0 & 0 & 0 \\ & & Q_{33} & 0 & 0 & 0 \\ & & & Q_{44} & 0 & 0 \\ & sym & & & Q_{55} & 0 \\ & & & & & Q_{66} \end{bmatrix} \cdot$$
$$\begin{bmatrix} \varphi_1 & 0 & 0 & 0 & 0 & 0 \\ 0 & \varphi_2 & 0 & 0 & 0 & 0 \\ 0 & 0 & \varphi_3 & 0 & 0 & 0 \\ 0 & 0 & 0 & \frac{\varphi_2+\varphi_3}{2} & 0 & 0 \\ 0 & 0 & 0 & 0 & \frac{\varphi_1+\varphi_3}{2} & 0 \\ 0 & 0 & 0 & 0 & 0 & \frac{\varphi_2+\varphi_3}{2} \end{bmatrix}^{-1} = \begin{bmatrix} \left(\frac{1}{\varphi_1}\right)^2 Q_{11} & \frac{1}{\varphi_1\varphi_2}Q_{12} & \frac{1}{\varphi_1\varphi_3}Q_{13} & 0 & 0 & 0 \\ & \left(\frac{1}{\varphi_2}\right)^2 Q_{22} & \frac{1}{\varphi_2\varphi_3}Q_{23} & 0 & 0 & 0 \\ & & \left(\frac{1}{\varphi_3}\right)^2 Q_{33} & 0 & 0 & 0 \\ & & & \left(\frac{2}{\varphi_2+\varphi_3}\right)^2 Q_{44} & 0 & 0 \\ & sym & & & \left(\frac{2}{\varphi_1+\varphi_3}\right)^2 Q_{55} & 0 \\ & & & & & \left(\frac{2}{\varphi_1+\varphi_2}\right)^2 Q_{66} \end{bmatrix} \tag{11}$$

where Q_{ij} (i, j=1,2,3) is the component of undamaged stiffness matrix. Ultimately, substitute Eq. (3) into Eq. (11), we obtain:

$$[C] = \begin{bmatrix} d_1^2 Q_{11} & d_1 d_2 Q_{12} & d_1 d_3 Q_{13} & 0 & 0 & 0 \\ & d_2^2 Q_{22} & d_2 d_3 Q_{23} & 0 & 0 & 0 \\ & & d_3^2 Q_{33} & 0 & 0 & 0 \\ & & & d_{23} Q_{44} & 0 & 0 \\ & sym & & & d_{31} Q_{55} & 0 \\ & & & & & d_{12} Q_{66} \end{bmatrix} \tag{12}$$

where d_1=1−ω_1, d_2=1−ω_2, d_3=1−ω_3, d_{23}=$(2d_2d_3/(d_2 + d_3))^2$, d_{31}=$(2d_1d_3/(d_1 + d_3))^2$, d_{12}=$(2d_1d_2/(d_1 + d_2))^2$

$$Q_{11} = \frac{(1-\mu_{23}\mu_{32})E_1}{1-\mu_{12}\mu_{21}-\mu_{23}\mu_{32}-\mu_{13}\mu_{31}-2\mu_{12}\mu_{23}\mu_{31}}, \quad Q_{22} = \frac{(1-\mu_{13}\mu_{31})E_2}{1-\mu_{12}\mu_{21}-\mu_{23}\mu_{32}-\mu_{13}\mu_{31}-2\mu_{12}\mu_{23}\mu_{31}},$$
$$Q_{33} = \frac{(1-\mu_{12}\mu_{21})E_3}{1-\mu_{12}\mu_{21}-\mu_{23}\mu_{32}-\mu_{13}\mu_{31}-2\mu_{12}\mu_{23}\mu_{31}}, \quad Q_{12} = \frac{(\mu_{21}+\mu_{23}\mu_{31})E_2}{1-\mu_{12}\mu_{21}-\mu_{23}\mu_{32}-\mu_{13}\mu_{31}-2\mu_{12}\mu_{23}\mu_{31}},$$
$$Q_{23} = \frac{(\mu_{32}+\mu_{12}\mu_{31})E_3}{1-\mu_{12}\mu_{21}-\mu_{23}\mu_{32}-\mu_{13}\mu_{31}-2\mu_{12}\mu_{23}\mu_{31}}, \quad Q_{44} = G_{23}, \quad Q_{55} = G_{31}, \quad Q_{66} = G_{12}.$$

where E, G and μ are the Young's modulus, shear modulus and Poisson's ratio, respectively.

2.2 Micro Damage Criteria

The modified 3D Hashin-type criteria and Von Mises criterion are used to detect the damage state of each of elements in fiber yarns and resin-rich matrix. The specified formations are shown as follows.

① Yarn breaking and fiber-matrix shear-out failure in direction 1:

$$\left(\frac{\sigma_{11}}{X\left(V_f,T\right)}\right)^2+\alpha\left(\frac{\sigma_{12}}{S_{12}\left(V_f,T\right)}\right)^2+\alpha\left(\frac{\sigma_{13}}{S_{13}\left(V_f,T\right)}\right)^2\geq 1 \tag{13}$$

② Matrix cracking and fiber-matrix shear-out failure in direction 2 (or 3):

$$\left(\frac{\sigma_{22}+\sigma_{33}}{Y\left(V_f,T\right)}\right)^2+\alpha\frac{\sigma_{23}^2-\sigma_2\sigma_3}{\left(S_{23}\left(V_f,T\right)\right)^2}+\alpha\left(\frac{\sigma_{12}}{S_{12}\left(V_f,T\right)}\right)^2+\alpha\left(\frac{\sigma_{13}}{S_{13}\left(V_f,T\right)}\right)^2\geq 1 \tag{14}$$

where $\sigma_{ij}(i,j=1,2,3)$ are the stress components in the material coordinate system; X, Y and S denote the tensile and shear strength at given temperature, respectively. α is the shear contribution factors.

③ Von Mises criterion:

$$\left(\sigma_{11}-\sigma_{22}\right)^2+\left(\sigma_{22}-\sigma_{33}\right)^2+\left(\sigma_{11}-\sigma_{33}\right)^2+6\left(\tau_{12}^2+\tau_{13}^2+\tau_{23}^2\right)^2\geq 2X_m(T) \tag{15}$$

where $X_m(T)$ is the tensile strength of matrix at given temperature. Furthermore, the foregoing criteria can be utilized in detecting the damaged state at various temperatures.

2.3 Stiffness Degradation Strategy

Since the engineering constants can be directly measured by test machine, the direct discount approach is performed by setting the elastic constants to a small value once the micro damage criteria are satisfied, where the influence of small value is equivalent to that of d_i according to the Eq. (12). The related discount strategy is listed in Table 1.

3 Material and Experiment

In this section, a 2.5D woven fabric with layer to layer angle-interlock structure was firstly investigated by experiment. Next, the proposed procedure will be used to analyze the damage behavior of this material under uniaxial tension in the warp and weft directions, respectively.

The material was manufactured using T300 fiber yarns, consisting of 3K filaments per bundle, and the resin matrix is QY8911-IV with a glass transition temperature 256 °C, and the related mechanical properties are shown in Table 2. A dimension of 600 mm×480 mm flat composite panel with fiber volume fraction of 51.62 % was manufactured by resin transfer molding (RTM) technique (Fig. 1a), and all of the specimens with nominal dimensions of

Table 1 Degradation method of component materials

Failure modes	Component materials	Degradation method			
		E_1	E_2/E_3	G_{12}/G_{13}	G_{23}
Yarn breaking in direction *L*	Warp yarn	0.2	0.2	0.2	0.2
Matrix cracking in direction *T*/*Z*		1	0.4	0.4	0.4
Yarn breaking in direction *L*	Weft yarn	0.2	0.2	0.2	0.2
Matrix cracking in direction *T*/*Z*		1	0.4	0.4	0.4
Pure resin matrix failure	matrix	0.4	0.4	0.4	0.4

300 mm×480 mm were cut from the panel by an abrasive water-jet cutting technique (see Fig. 1b). Additionally, the woven parameters are listed in Table 3.

All of the specimens were conducted by an MTS 810 test machine with a 25.4 mm MTS-634-25 extensometer used to monitor the strain continuously during the static tests under warp and weft tensile loading. Additionally, all of the static experiments were completed under displacement control at a constant rate of 0.5 mm/min in compliance with test standard ASTM D 3039 [12] Fig. 2.

4 Simulation and Discussion

In order to verify the validity of this method with finite element technology, two kinds of FE models with/without outmost layer structure have been established in the Part I by this author, and the corresponding FE models are directly illustrated in Fig. 3. Additionally, the periodic boundary condition for these two models has been investigated in the Part I in detail. Thus the key simulation results will be directly shown in this Part.

4.1 Uniaxial Tension in the Warp Direction

A set of six specimens were performed in the warp direction at room temperature. The related stress–strain curves for typical specimens are plotted in Fig. 3.

According to the Fig. 3a, it can be clearly observed that the experimental curve experiences a linear behavior initially until to the state in which the strain is approximately equivalent to 1.0 %, followed by an obvious nonlinear characteristic up to failure. Additionally, good coincidence between experimental curve and predicted curve based on the Full-cell model has been obtained. It is indicated that the proposed approach is available to describe the damage behavior and predict the static strength of 2.5D woven composites, precisely. The predicted curve referred to the Inner-cell model shows a

Table 2 Mechanical properties of fiber and matrix in 2.5D woven composites

	E_{f1}/Em	E_{f2}	G_{f12}/G_m	G_{f23}	u_{f12}/u_m
T300-3K	230	40	17	4.8	0.3
QY8911-IV	4.16	–	–	–	0.34

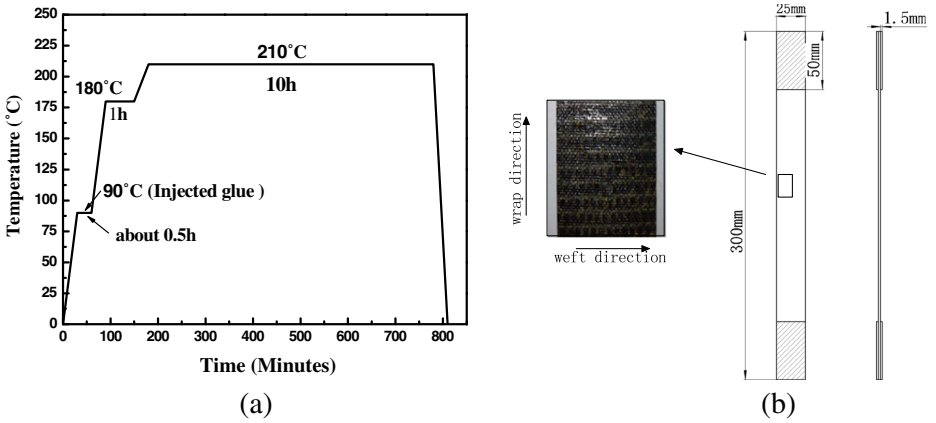

Fig. 1 The diaphragm-curing process (**a**) and photograph of specimens (**b**)

higher mechanical behavior than that based on the Full-cell model in comparison with the test curve, which may be attributed to the fact that the periodic distribution along the direction of thickness is not satisfied.

The damage situation of 2.5D woven composites under the static loading in the warp direction is quantitatively grasped as illustrated in Fig. 3b. From the Fig. 3b, it can be clearly seen that the relatively critical stiffness discount, appeared in point A, is due to the matrix cracks in the warp and failure in resin-rich parts. After that, more and more damages are occurred as the strain increase, which ultimately causes the overall failure of specimen is reached. A mount of yarn transverse damages, failure damages in resin-rich part and yarn longitudinal damages have been quantitatively counted, which ultimately causes the occur of failure of 2.5D woven composites. The damage evolution processes of each component are in detail illustrated in Figs. 4, 5, and 6, in which the loading direction is parallel to X-axis (warp direction as well) that is shown in Fig. 2.

In the warp tensile process shown in Figs. 4, 5, and 6, transverse cracks in the warp yarns occur initially at the cross-over regions between warp and weft yarns (see Fig. 4). Afterwards, the cracks progress in the warp yarns along the weft direction. When the loading strain grows up to 0.8 %, the yarn longitudinal damages can be found in the inclination segment of warps, which to some extent give rise to the reduction of load (Fig. 3a). From this point onwards, amount of yarn longitudinal damages are propagated along the weft direction, during which the stress–strain response presents an obvious nonlinear behavior up to the peak point. Ultimately, the failure of the 2.5D woven

Table 3 Woven parameters of specimens

Wrap arranged density M_f(tows/cm)	Weft arranged density M_w(tows/cm)	Number of weft yarn at the same height N_f	Number of layers in weft direction N_h	Height Lz(mm)	Packing factor of fiber in wrap yarn Pj
10	3.5	5	6	1.95	0.765

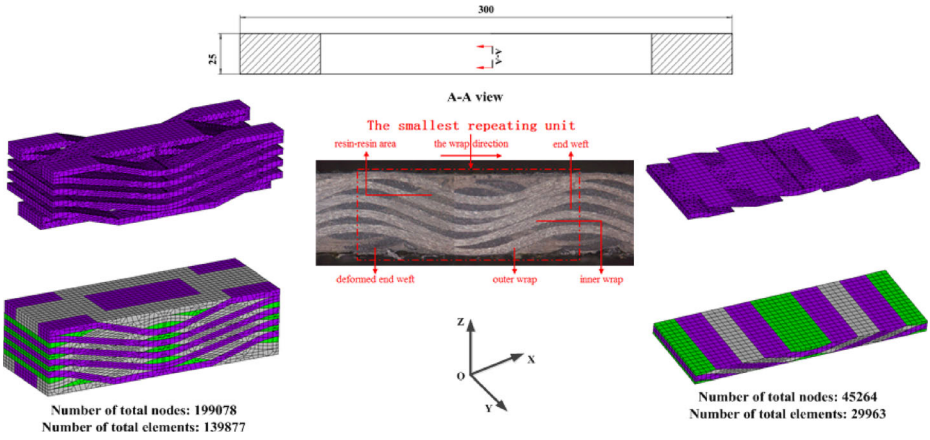

Fig. 2 Three-dimensional FE model for 2.5D woven carbon fabric composites

composites subjected to the static tensile loading in the warp direction is occurred, which is mainly due to the yarn longitudinal cracks propagated to the boundary of structure (Fig. 4). Additionally, a certain degree of matrix cracks and transverse damages in the weft yarns are observed, but no longitudinal damages in weft yarns are found (Figs. 5 and 6).

To investigate the fractured surface morphology, Fig. 7 presents the fractured surface of the specimen under tensile loading in the warp direction. It can be found that the fracture mainly occurs in the inclined segments of warp fiber bundles, which is similar with the simulation results as shown in Fig. 4. The fractured plane of each bundle is not co-planar (Fig. 7c), but relatively integrate (Fig. 7d), which indicates that the finial failure results from the warp yarns breaking damage mode. Additionally, a certain degree of delamination cracks and transverse damages in the weft yarns can be observed around the fracture regions. Furthermore, amount of warp yarns breaking damages manifest that this is a brittle-natured material.

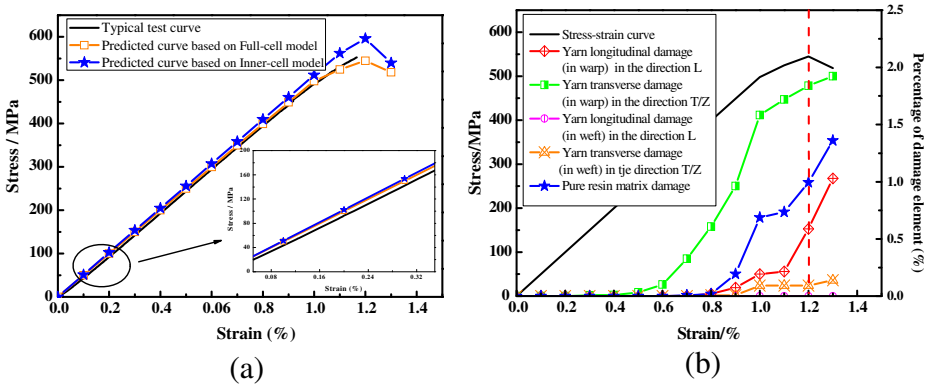

Fig. 3 **a** Compared results and **b** damage cumulative process under static tension in the warp direction

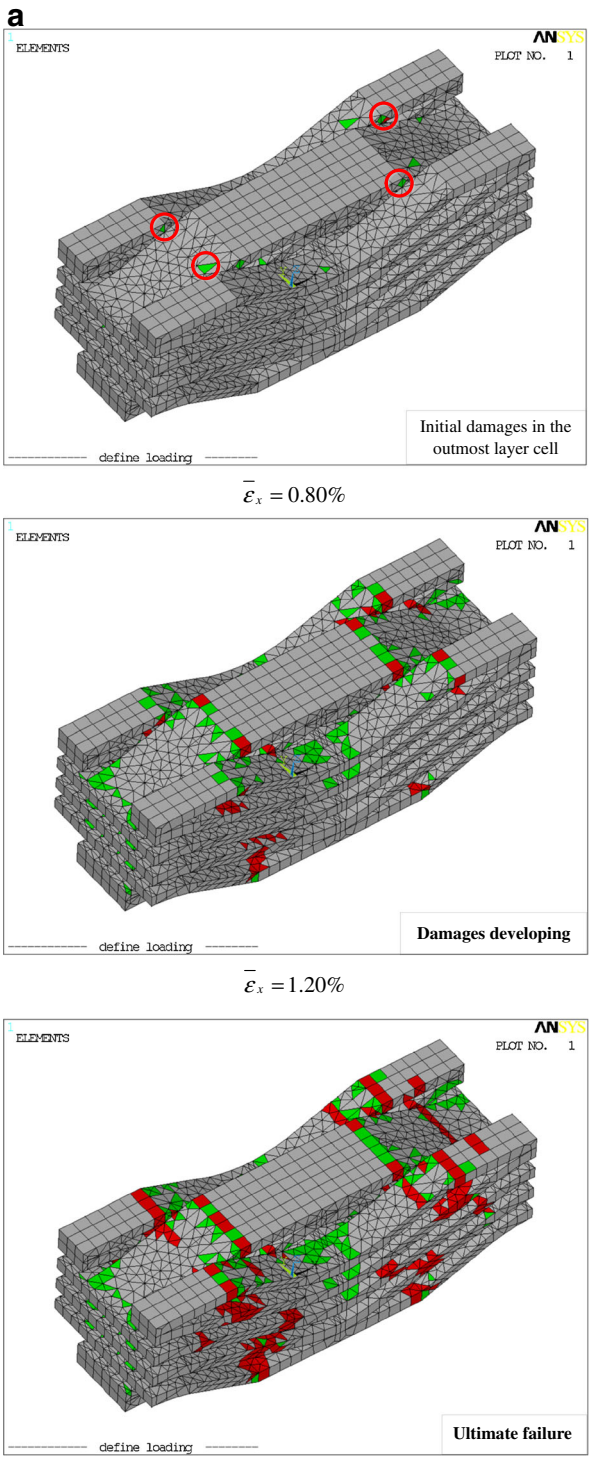

Fig. 4 **a** Damage development process in the warp yarns under warp tensile loading based on the Full-cell model. **b** Damage development process in the warp yarns under warp tensile loading based on the Inner-cell model

Fig. 4 (continued)

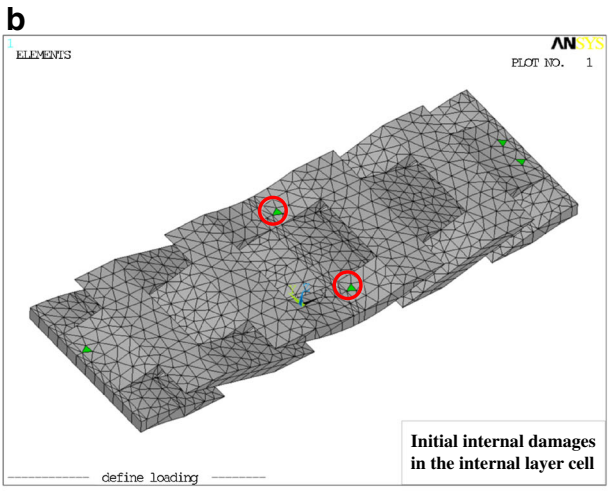

$\bar{\varepsilon}_x = 1.20\%$

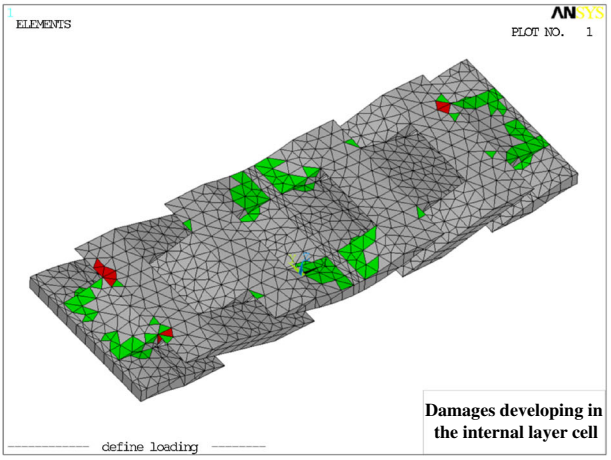

$\bar{\varepsilon}_x = 1.40\%$

4.2 Uniaxial Tension in the Weft Direction

The contrasting results between computational and experimental stress–strain curves of 2.5D woven composites under static tension in the weft direction are shown in Fig. 8a. It is noticed that the experimental stress–strain behavior in a bilinear manner as the load in the weft direction increases. A certain extent of deviation is observed for the prediction curves, which reflects in that there is not an obvious nonlinear change in the stress–strain curve, especially the curve obtained based on the Inner-cell model. Additionally, the prediction curve based on the Full-cell model is greater than that based on the Inner-cell model owing to the periodic boundary condition. As the damages increase, the structure does not fully meet the periodic condition, which inevitable leads to the higher prediction results based on simulation approach.

Fig. 5 **a** Damage development process in the weft yarns under warp tensile loading based on the Full-cell model. **b** Damage development process in the weft yarns under warp tensile loading based on the Inner-cell model

a

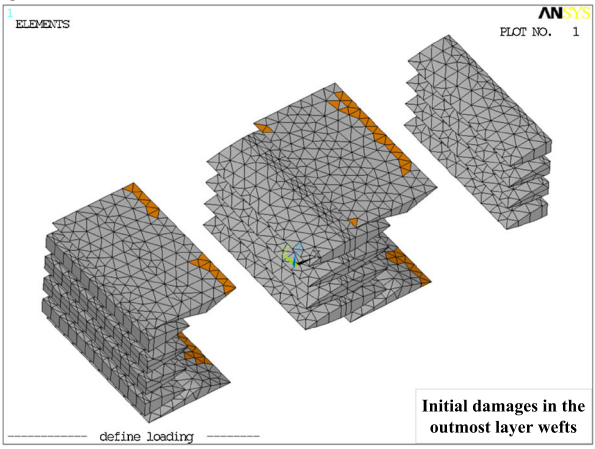

$\bar{\varepsilon}_x = 1.20\%$

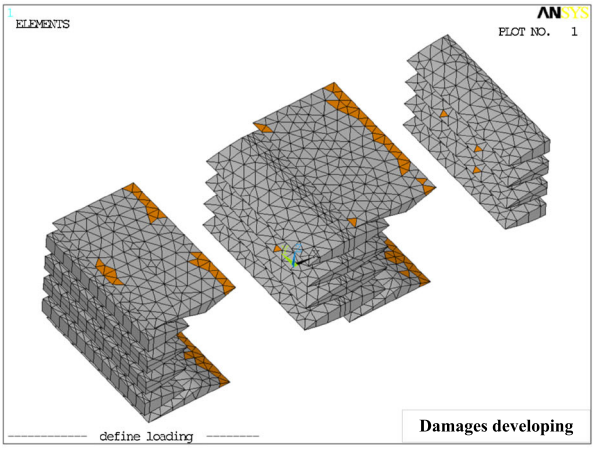

$\bar{\varepsilon}_x = 1.30\%$

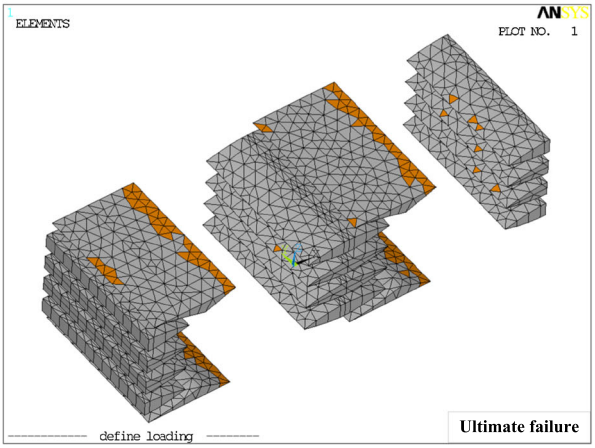

$\bar{\varepsilon}_x = 1.40\%$

Fig. 5 (continued)

b

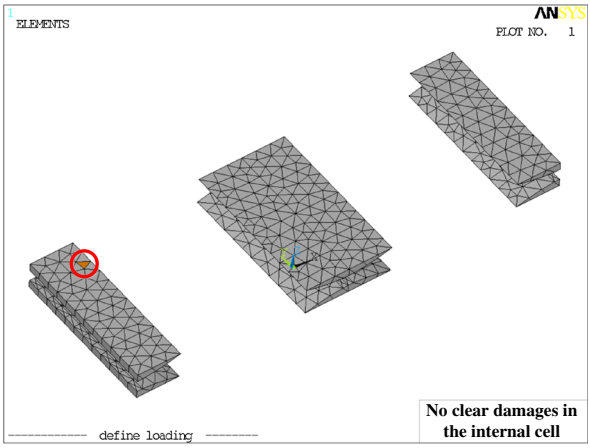

$\bar{\varepsilon}_x = 1.20\%$

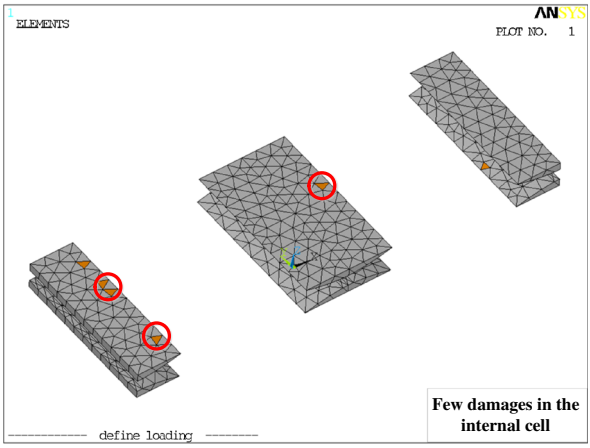

$\bar{\varepsilon}_x = 1.30\%$

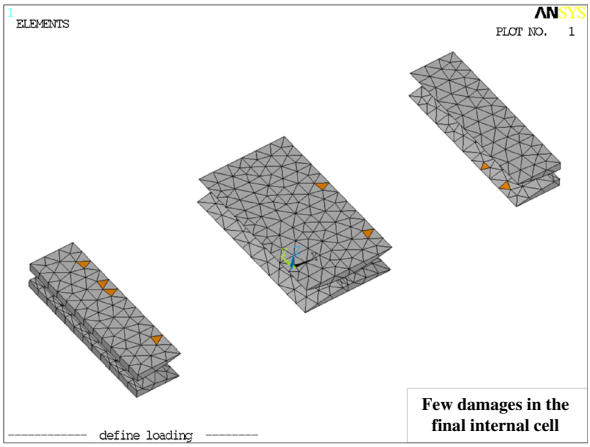

$\bar{\varepsilon}_x = 1.40\%$

Fig. 6 **a** Progressive damage process of resin-rich matrix under uniaxial tension in warp direction based on the Full-cell model. **b** Progressive damage process of resin-rich matrix under uniaxial tension in warp direction based on the Inner-cell model

a

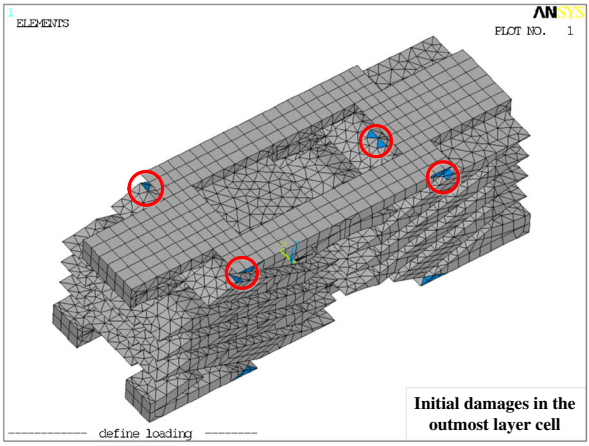

$\bar{\varepsilon}_x = 0.09\%$

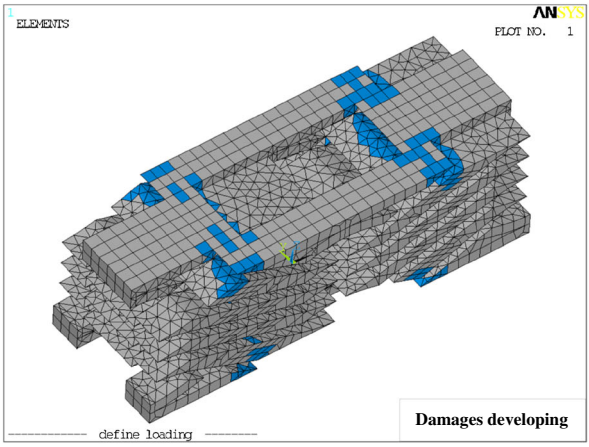

$\bar{\varepsilon}_x = 1.20\%$

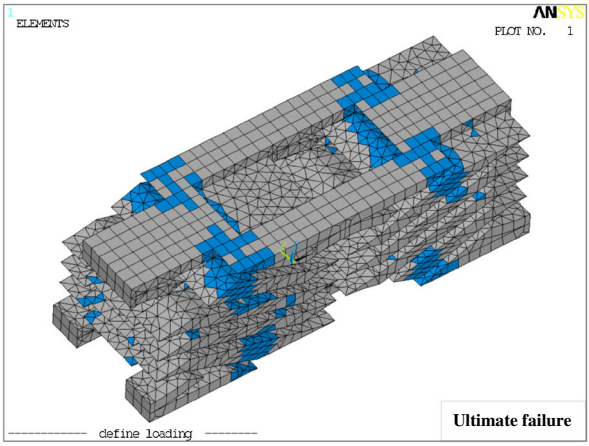

$\bar{\varepsilon}_x = 1.40\%$

Fig. 6 (continued)

b

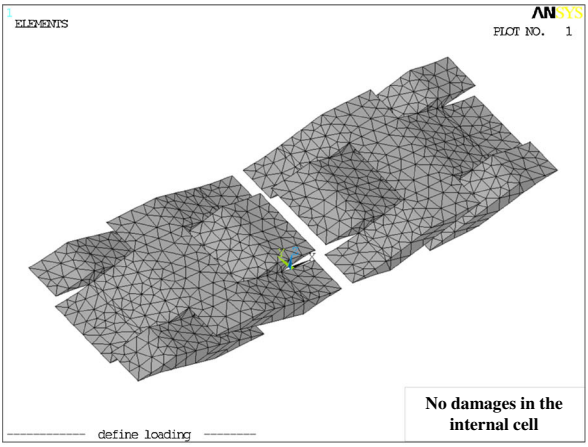

$\bar{\varepsilon}_x = 0.09\%$

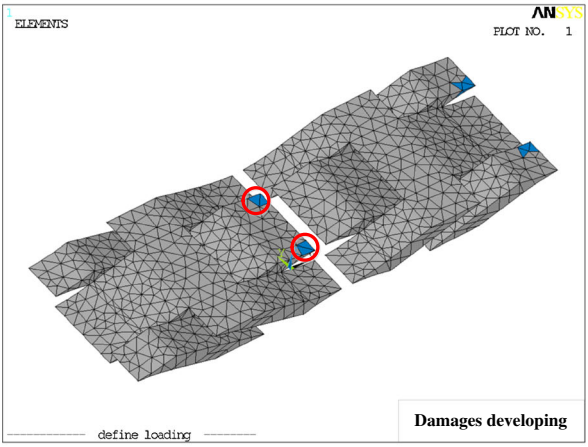

$\bar{\varepsilon}_x = 1.20\%$

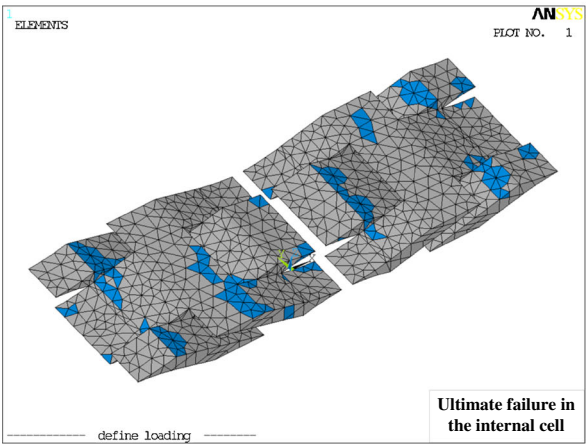

$\bar{\varepsilon}_x = 1.40\%$

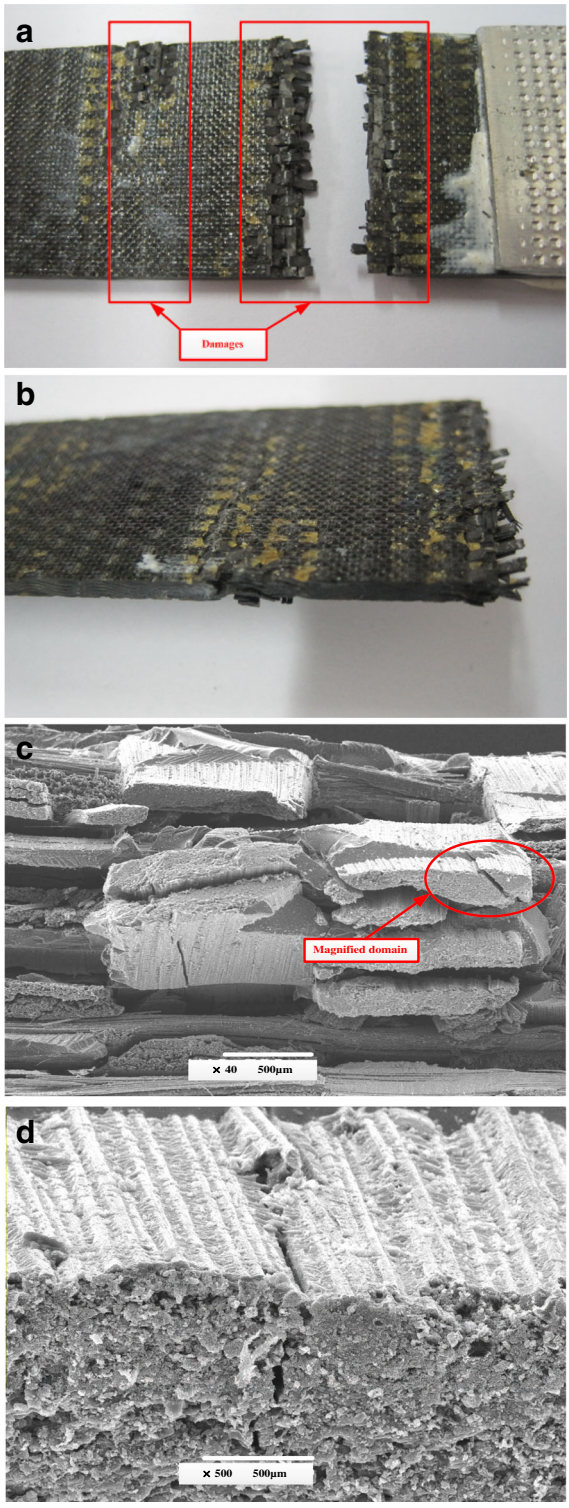

Fig. 7 **a** Photograph of fracture surface subjected to warp loading shot by photos (*Top view*). **b** Photograph of fracture surface subjected to warp loading shot by photos (*Lateral view*). **c** SEM photomicrograph of fracture surface subjected to warp loadings (×40). **d** SEM photomicrograph of fracture surface subjected to warp loadings (×500)

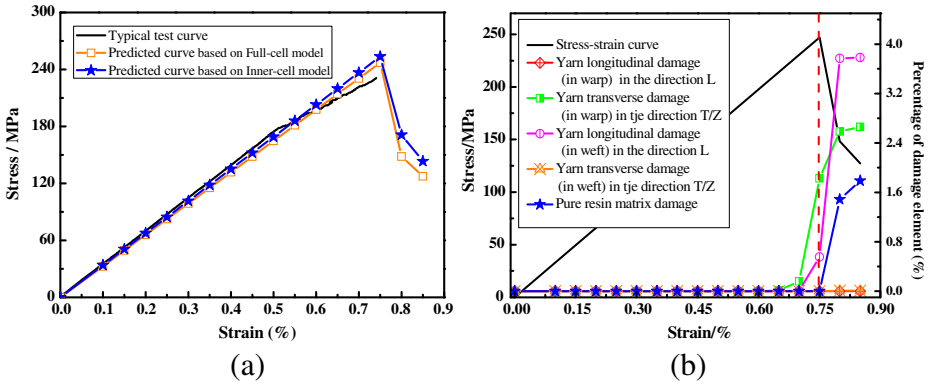

Fig. 8 **a** Compared results and **b** damage cumulative process under static tension in the warp direction

Figure 8b shows the percentage of damage elements vs. strain curve of 2.5D woven composites based on the Full-cell model, and the corresponding detailed damage process is illustrated in Figs. 9, 10, and 11, in which the load direction is parallel to Y-axis (weft direction as well). According to the Fig. 8b, it is manifest that the yarn longitudinal damages in weft yarns make greater contribution to eventually failing of the composites.

During the loading process, the yarn transverse cracks are firstly observed at the cross-over zones of the warp and weft yarns (Figs. 9a and 10a). After that, more transverse cracks occur at the cross-over zones, and progress along the path perpendicular to the load, which triggers the appearance of yarn longitudinal damages in the outmost layer weft yarns and matrix damages. With the load increasing, the yarn longitudinal cracks propagate sharply to the internal weft yarns within 0.5 % strain from 0.75 to 0.8 % (Fig. 9). Therefore, the longitudinal cracks cross through the whole weft yarn sections, which ultimately causes that the stress–strain curve experiences a rapid fall from 247 MPa in 0.75 % strain to 148 MPa in 0.8 % strain (Fig. 9). Additionally, the failure elements in rich-resin parts are quite few, and the fracture surfaces are obviously perpendicular to the loading direction (Fig. 11).

Figure 12 displays the fracture surface of the specimen failed under tensile load in the weft direction. It can be clearly found that the fracture surface is remarkable even and no necking phenomenon is observed. Compared to the simulation results shown in Figs. 9, 10, and 11, good coincidence in the failure surface morphology is observed, which evidences that the simulation approach proposed by this author can be used to simulate the mechanical behavior and predict the mechanical performance.

4.3 Discussion on the Mechanical Performance

Owing to the existing of fabrication and measurement errors, the influence of woven parameters on the mechanical performance will be discussed in this section. Figure 13 presents the change of the stress–strain curves based on the Full-cell model under tensile load in the warp or weft direction with the woven parameters, including the thickness (L_z), warp arranged density (M_j) and weft arranged density (M_w).

In general, it can be clearly observed from Fig. 13 that the woven parameters (L_z, M_j and M_w) have a greater influence on the stress–strain curves under the warp tensile load than the

Fig. 9 **a** Damage process of weft under the weft loading based on the Full-cell model. **b** Damage process of weft under the weft loading based on the Inner-cell model

a

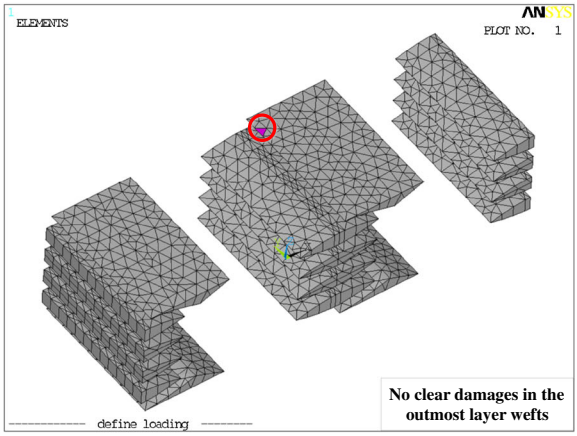

$\bar{\varepsilon}_y = 0.70\%$

$\bar{\varepsilon}_y = 0.08\%$

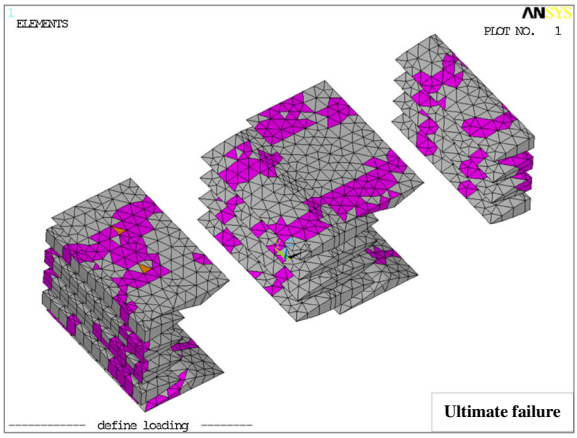

$\bar{\varepsilon}_y = 0.85\%$

Fig. 9 (continued)

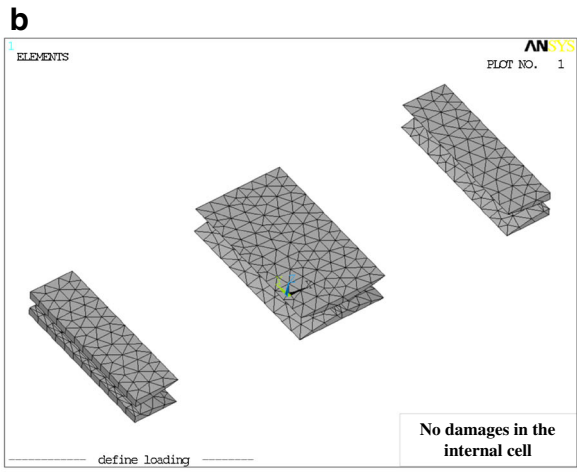

$\bar{\varepsilon}_y = 0.70\%$

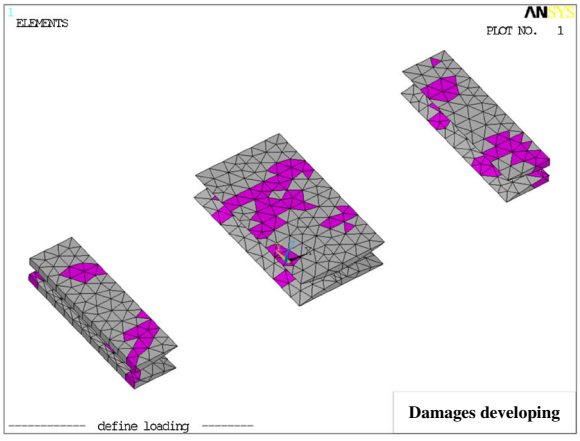

$\bar{\varepsilon}_y = 0.80\%$

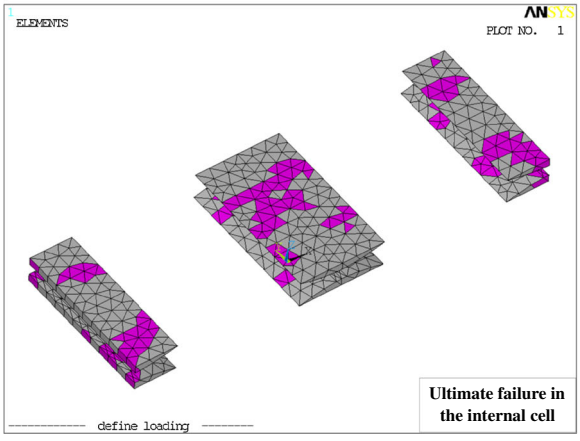

$\bar{\varepsilon}_y = 0.85\%$

Fig. 10 **a** Damage process of warp under the weft loading based on the Full-cell model. **b** Damage process of warp under the weft loading based on the Inner-cell model

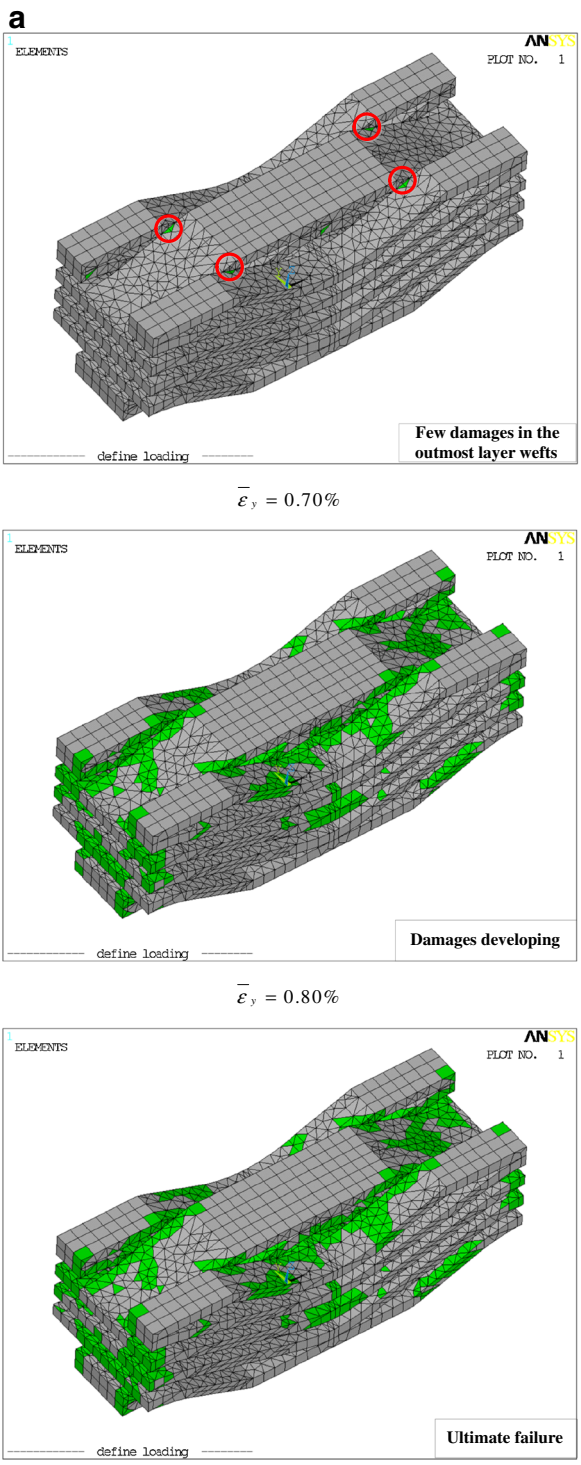

Fig. 10 (continued)

b

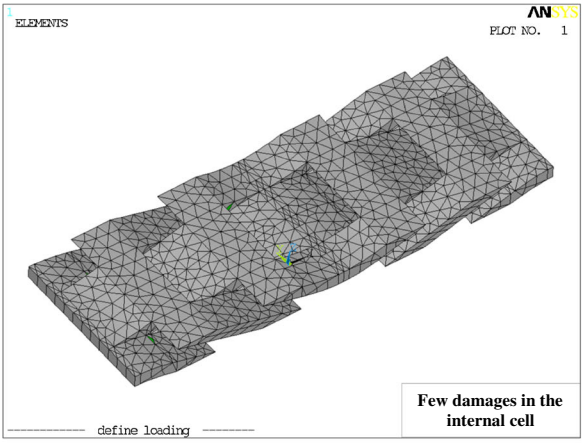

$\bar{\varepsilon}_y = 0.70\%$

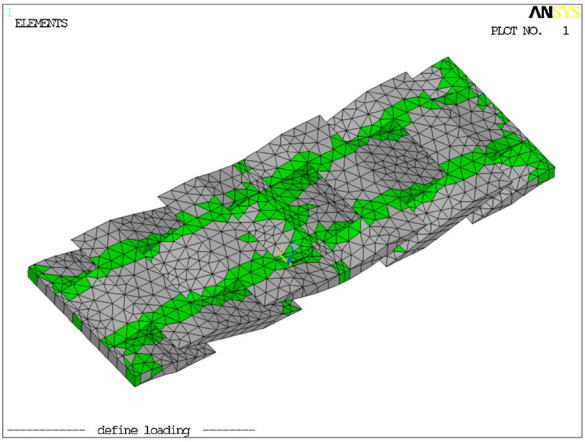

$\bar{\varepsilon}_y = 0.80\%$

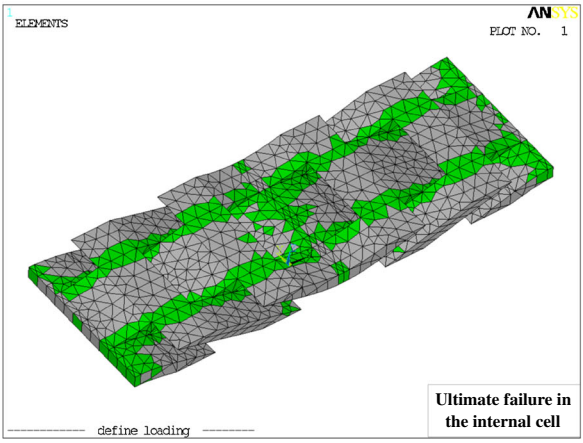

$\bar{\varepsilon}_y = 0.85\%$

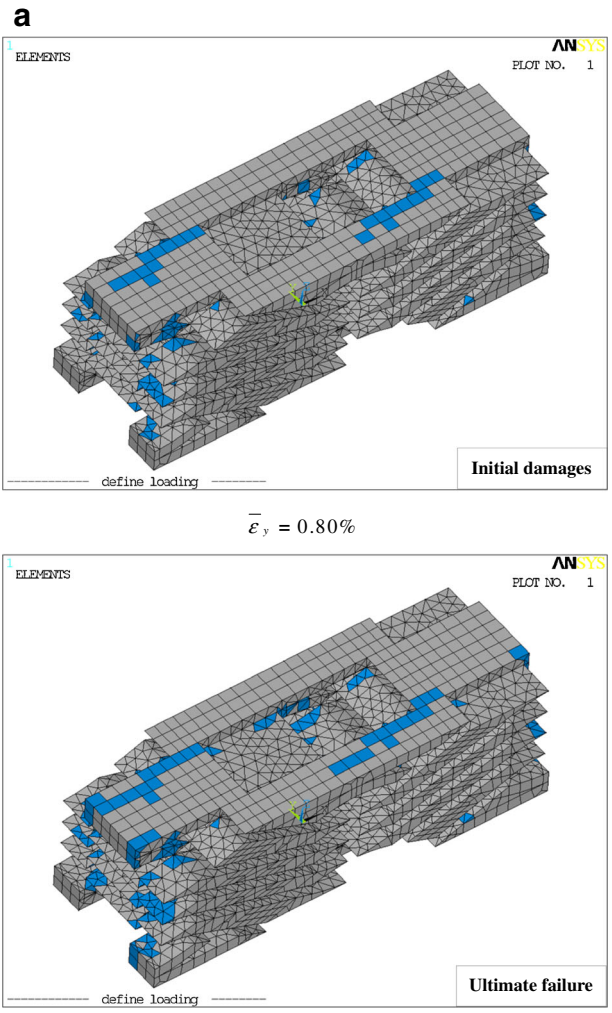

Fig. 11 **a** Damage process of resin-rich matrix under the weft loading based on the Full-cell model. **b** Damage process of resin-rich matrix under the weft loading based on the Inner-cell model

corresponding curves under the weft tensile load. To be more specific, as the L_z increases, the strength in the warp direction at the thickness of 2.03 mm drops by 6.33 % of the related strength at 1.87 mm, whereas the strength in the weft direction remains stable, just declining by 2.12 % (Fig. 13a and b).

From the Fig. 13c and d, the stress–strain curves referred to the warp tension have a significant decrease trend with the increase of M_j. In contrast, the corresponding curves subjected to the weft tension see an opposite trend. Likewise, in terms of the impact of M_j on the mechanical behavior, it can be seen from the Fig. 13e and f that there the variety of stress–strain curves under the warp tensile load affected by Mw exhibits an opposite trend with that of stress–strain curves subjected to the weft load.

b

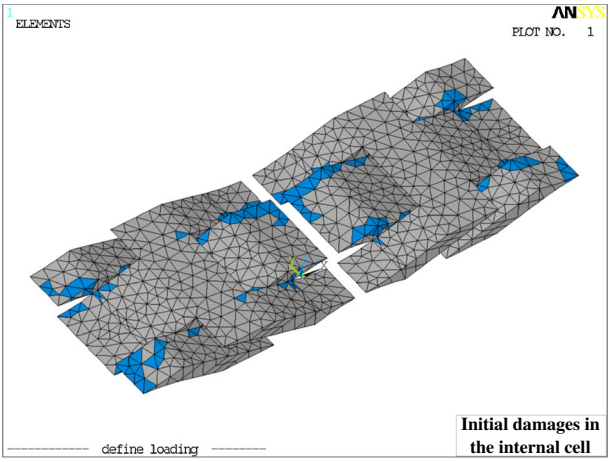

$\bar{\varepsilon}_y = 0.80\%$

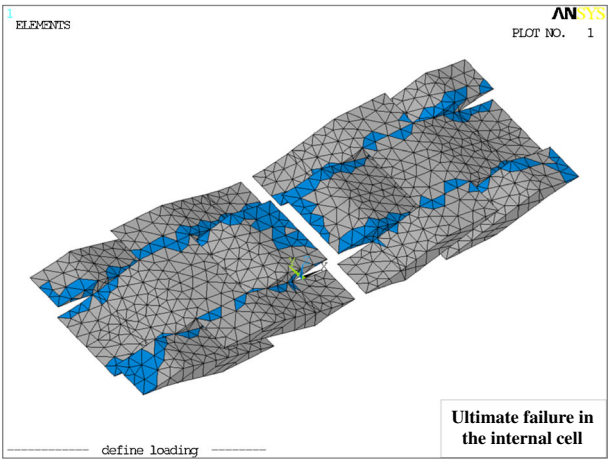

$\bar{\varepsilon}_y = 0.85\%$

Fig. 11 (continued)

5 Conclusions

The detailed numerical investigation based on the Full-cell model on the mechanical behavior of 2.5D woven composites subjected to uniaxial tensile load in the warp and weft directions has been presented. According to the simulation results, some useful conclusions can be drawn as follows:

(1) The proposed progressive damage approach based on damage mechanics can simulate the damage accumulation accurately and failure modes of composites subjected to the warp (or the weft) load. Additionally, the predictive stress–strain curve under uniaxial load in the warp (or the weft) direction based on the Full-cell model is superior to that based on the Inner-cell model.

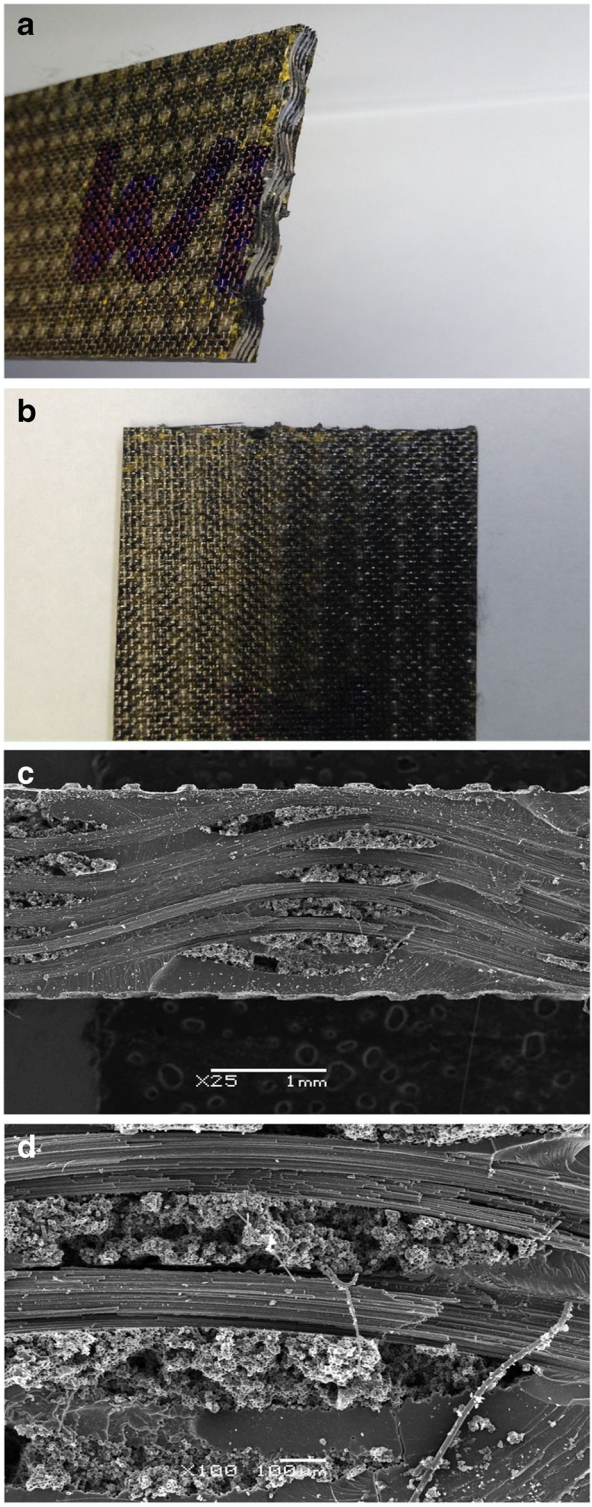

Fig. 12 **a** Photographs of fracture surface subjected to weft loadings shot by photos (*Side view*). **b** Photographs of fracture surface subjected to weft loadings shot by photos (*Top view*). **c** SEM photomicrograph of fracture surface subjected to warp loadings (×25). **d** SEM photomicrograph of fracture surface subjected to warp loadings (×100)

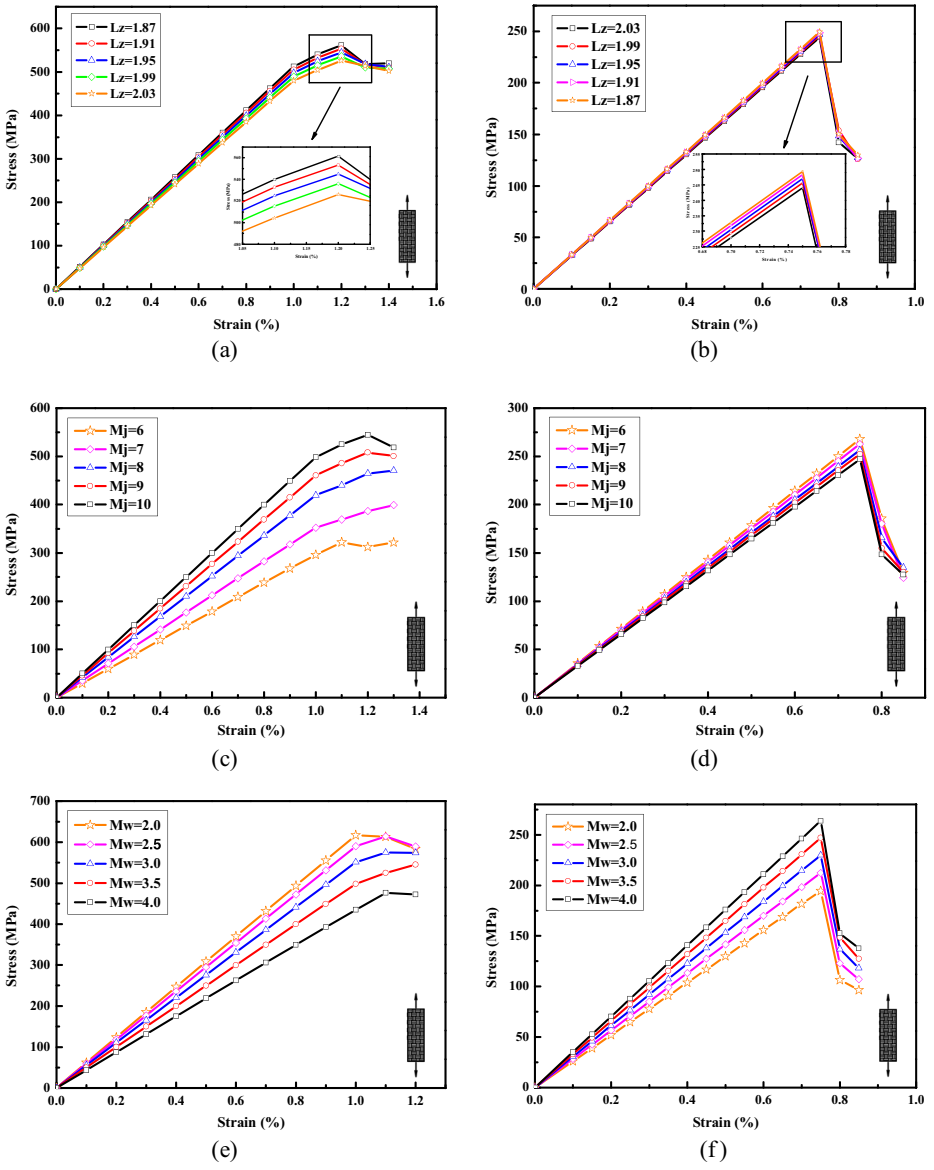

Fig. 13 Variation of the stress–strain curves with the thickness, warp arranged density and weft arranged density (**a**), (**b**)

(2) The initial cracks can be observed at the face structure under the tensile load in the warp (or the weft) directions, and the evolution path of cracks is perpendicular to the related loading direction. The main failure mode of 2.5D woven composites in the warp (or the weft) direction is the yarn breaking mode.

(3) The tensile strength in the warp (or the weft) direction declines with the thickness increases. However, the influence of M_j (or M_w) on the strength in the warp and weft shows an opposite trend.

Acknowledgments The work was supported by Jiangsu Innovation Program for Graduate Education [grant number KYLX_0237].

Compliance with Ethical Standards All authors have read and approved this version of the article, and due care has been taken to ensure the integrity of the work. Neither the entire paper nor any part of its content has been published or has been accepted elsewhere. It is not being submitted to any other journal. We wish the paper may be of particular interest to the readers of your journal.

References

1. Hallal, A., Younes, R., Fardoun, F., et al.: Improved analytical model to predict the effective elastic properties of 2.5 D interlock woven fabrics composite[J]. Compos. Struct. **94**(10), 3009–3028 (2012)
2. Jiang, Y., Tabiei, A., Simitses, G.J.: A novel micromechanics-based approach to the derivation of constitutive equations for local/global analysis of a plain-weave fabric composite[J]. Compos. Sci. Technol. **60**(9), 1825–1833 (2000)
3. Ishikawa, T., Chou, T.: Elastic behavior of woven hybrid composites[J]. J. Compos. Mater. **16**(1), 2–19 (1982)
4. Zheng, J.: Research on elastic property prediction and failure criteria of 2.5D woven composites[D]. Nanjing University of Aeronautics and Astronautics, Nanjing (2008)
5. Selezneva, M., Montesano, J., Fawaz, Z., et al.: Microscale experimental investigation of failure mechanisms in off-axis woven laminates at elevated temperatures[J]. Compos. A: Appl. Sci. Manuf. **42**(11), 1756–1763 (2011)
6. Vieille, B., Taleb, L.: About the influence of temperature and matrix ductility on the behavior of carbon woven-ply PPS or epoxy laminates: Notched and unnotched laminates[J]. Compos. Sci. Technol. **71**(7), 998–1007 (2011)
7. Zako, M., Uetsuji, Y., Kurashiki, T.: Finite element analysis of damaged woven fabric composite materials[J]. Compos. Sci. Technol. **63**(3), 507–516 (2003)
8. Lu, Z., Zhou, Y., Yang, Z., et al.: Multi-scale finite element analysis of 2.5 D woven fabric composites under on-axis and off-axis tension[J]. Comput. Mater. Sci. **79**, 485–494 (2013)
9. Dong, W.F., Xiao, J., Li, Y.: Finite element analysis of the tensile properties of 2.5 D braided composites[J]. Mater. Sci. Eng. A **457**(1), 199–204 (2007)
10. Li, D., Li, J., Chen, L., et al.: Finite element analysis of mechanical properties of 3D four-directional rectangular braided composites part 1: Microgeometry and 3D finite element model[J]. Appl. Compos. Mater. **17**(4), 373–387 (2010)
11. Jiwei, D., Miaolin, F.: Damage simulation for 3D braided composites by homogenization method[J]. Chin. J. Aeronaut. **23**(6), 677–685 (2010)
12. Astm International A: D3039: Standard test method for tensile properties of polymer matrix composite materials[J]. ASTM International, West Conshohocken (2000)